Shear moduli in bcc-fcc structure transition of colloidal crystals

Hongwei Zhou, Shenghua Xu, Zhiwei Sun, and Ruzeng Zhu

Citation: The Journal of Chemical Physics **143**, 144903 (2015); doi: 10.1063/1.4932684
View online: http://dx.doi.org/10.1063/1.4932684
View Table of Contents: http://scitation.aip.org/content/aip/journal/jcp/143/14?ver=pdfcov
Published by the AIP Publishing

Shear moduli in bcc-fcc structure transition of colloidal crystals

Hongwei Zhou,[1] Shenghua Xu,[1,a)] Zhiwei Sun,[1] and Ruzeng Zhu[1,2]
[1]*Key Laboratory of Microgravity (National Microgravity Laboratory), Institute of Mechanics, Chinese Academy of Sciences, Beijing 100190, China*
[2]*State Key Laboratory of Nonlinear Mechanics, Institute of Mechanics, Chinese Academy of Sciences, Beijing 100190, China*

(Received 18 June 2015; accepted 28 September 2015; published online 9 October 2015)

Shear moduli variation in the metastable-stable structure transition of charged colloidal crystals was investigated by the combination techniques of torsional resonance spectroscopy and reflection spectrometer. Modulus of the system increases with the proceeding of the transition process and it finally reaches the maximum value at the end of the transition. For colloidal crystals in stable state, the experimental moduli show good consistence with theoretical expectations. However, in the transition process, the moduli are much smaller than theoretical ones and this can be chalked up to crystalline imperfection in the transition state. © *2015 AIP Publishing LLC.* [http://dx.doi.org/10.1063/1.4932684]

I. INTRODUCTION

Colloidal crystals, owing to their unique easily accessible time and length scales, are usually considered as ideal model systems of atomic or molecular systems for studying the nucleation behavior, crystal growth, and phase transition and evaluating some classic theories.[1–5] Furthermore, the periodic modulation of the refractive index makes it to be an attractive material, photonic crystals, having potential applications in optical fibers, displays, and sensors.[6–8]

For charged colloidal systems consisting of submicrometer particles and the surrounding medium, one great advantage is that the interparticle interaction potential can be tuned conveniently through particles surface charge, number density, and electrolyte concentration. Depending on the strength and range of the interaction, colloidal suspensions show a variety of different phases as fluid, solid crystals with crystal lattice structures as body-centered cubic (bcc) or face-centered cubic (fcc), and even glassy morphology.[9–11] Besides the common spherical particles, systems composed of particles with other geometries like rods,[12,13] ellipsoids,[14,15] or cubes[16,17] were also studied recently, and some new fascinating phase behaviors have been found.

On the other hand, crystallization kinetics of colloidal particles, including homogeneous and heterogeneous nucleation and growth process, conducted in the well-characterized systems were broadly investigated with the aid of some improved experimental technologies.[18–20] It was found that classical nucleation theory (CNT) and Wilson-Frenkel law, which is usually used in atomic and molecular systems, are also applicable in colloidal crystallization though some challenges were found under some specific conditions.[4,21] Recently, the validity of the classic Ostwald's step rule (conceived by Wilhelm Ostwald as an empirical rule) has also been verified in experiments and computer simulations in colloidal crystallization.[22–25] This step rule states that in general it is not the most stable but the least stable polymorph that crystallizes first. This stepwise crystallization phenomenon usually causes crystals with different structures before they reach the final stable state. And correspondingly the properties of the systems will also change because each polymorph has its specific optical (or electrical) and other physical properties. For a simplest example, both diamond and graphite have the same chemical composition but different structures make them show completely different physical properties.

Shear modulus G is a basic physical parameter characterizing the rigidity of colloidal crystals. Generally, it is determined by crystal lattice structures and experimental parameters that influence the interparticle interaction, such as number density n or salt concentration C_{salt}.[26–28] For example, G of crystals with bcc structure are always larger than that of fcc under the same number density and G decreases with increasing C_{salt} and decreasing n. Actually, in addition to crystal lattice structures and interparticle interaction mentioned above, there are also some other factors that influence the modulus. Palberg *et al.* found morphology and texture have significant influences to modulus, and the moduli of crystals with preferential orientation (prepared by shear processing) are much lower than that of crystals with random orientation.[29] Schöpe *et al.* found, when crystals change from polycrystalline to nanocrystalline with increasing n, the experimentally obtained moduli are always larger than theoretical expectations.[30] Therefore, all these findings indicate that moduli of colloidal crystals are the synergetic result of various factors.

However, the studies in the literatures mainly focus on the equilibrium state, there is little known about moduli variation in the non-equilibrium process, such as structure transition. The aim of this study is to explore how G evolves in the bcc-fcc transition. Meanwhile, because in microscopic level G is related with interparticle interaction and it has been found that theoretical formulas deduced from screened Coulomb

a)Author to whom correspondence should be addressed. Electronic mail: xush@imech.ac.cn. Tel.: +86 10 82544099. Fax: +86 10 82544096.

potential can satisfactorily explain the experimental results in a quantitative manner, we are expecting the present study would provide some useful information for better understanding the mechanism of bcc-fcc transition.

Particularly, however, the magnitude of G of colloidal crystals is very small due to their extremely low particle concentration, and the crystals can be easily destroyed by even slightly mechanical perturbations, which make traditional direct mechanical measurements unsuitable. To measure G, torsional resonance spectroscopy (TRS) technique has been adopted as that reported in the literatures (more about this approach will be described in Sec. II).[29–32] Through tuning the range of frequency swept and the structure transition rate, enough time resolution can be guaranteed. Additionally, in the transition process crystal lattices keep changing and therefore how to promptly determine the crystal lattice structures is another key problem. Taking advantage of the newly developed reflection spectrometer (RS) technique to fast identify the crystal lattice structures, we can solve this problem (now the sample rate of RS can be up to 100 times/s, namely, only 0.01 s is needed).

In this study, RS is combined with TRS to simultaneously monitor the crystal lattice structures and moduli variation of colloidal crystals in the whole transition process from bcc to fcc. We found G increases when the crystals change from metastable bcc to stable fcc. And G of both stable bcc and stable fcc have good consistence with theoretical expectations, but G in the transition process from bcc to fcc are much smaller than theoretical ones.

II. EXPERIMENTS

A. Materials

Polystyrene (PS) particles synthesized by emulsion-free polymerization were used in this study. Sulfate groups bonded chemically on the particle surface dissociate in solution, which results in electrical double layer surrounding the particles. The diameter and polydispersity of the particles were measured in 1 mM sodium chloride solution by means of dynamic light scattering (DLS, Brookhaven Instruments Corp., USA). The diameters are 105 nm and 98 nm, and the polydispersities are 0.034 and 0.048, both smaller than 5%. For convenience the two batches of PS particles are designated as PS105 and PS98. The effective charge numbers determined by modulus measurements (details see Section III C below) are approximately 400 ± 26 for PS105 and 440 ± 40 for PS98, respectively.

B. Experimental setup

The experimental setup used in this study was shown in Fig. 1. It mainly contains three parts from top to bottom: sample preparation unit, reflection spectrometer, and torsional resonance spectroscopy. For each part, its functionality and components are described below.

1. Sample preparation unit

This part is used to deionize the colloidal suspensions and to regulate the particle concentration. Similar to that reported in our previous papers and other groups,[22,29] it contains two peristaltic pumps (Masterflex, Cole-Parmer), a reservoir, an ion-exchange resin (G501-X8(D), Bio-Rad Laboratories) chamber, and a conductivity measurement unit (DDS-12A, Shanghai Pengshun Scientific Instrument Co., Ltd.). All the units are connected by tubes to form a circulation system. First, both pump 2 and pump 1 are shut down and colloidal suspensions with known concentration are added to the reservoir, and then pump 1 is turned on to circulate the suspensions to pass through ion-exchange resin. The conductivity of the suspensions is measured by conductivity meter. After the suspensions are fully deionized, which is characterized by the conductivity is no longer decreased, pump 1 is shut down. And then pump 2 is turned on to circulate the suspensions into the cylindrical tube immersed in a constant temperature water bath for further observation. The concentration of the particles can be conveniently adjusted by adding latex or pure water, and the exact concentration can be evaluated through the conductivity measurements.[30,33]

2. Reflection spectrometer

A tungsten halogen light source (Avalight-HAL, Avantes) with available wavelength from 400 nm to 1000 nm was used to illuminate the polycrystalline sample in the tube through a "Y" type optic cable, and the reflected light through the same cable is detected by the optic spectrometer (Avaspec-2048, Avantes). The functionality of reflection spectrometer is

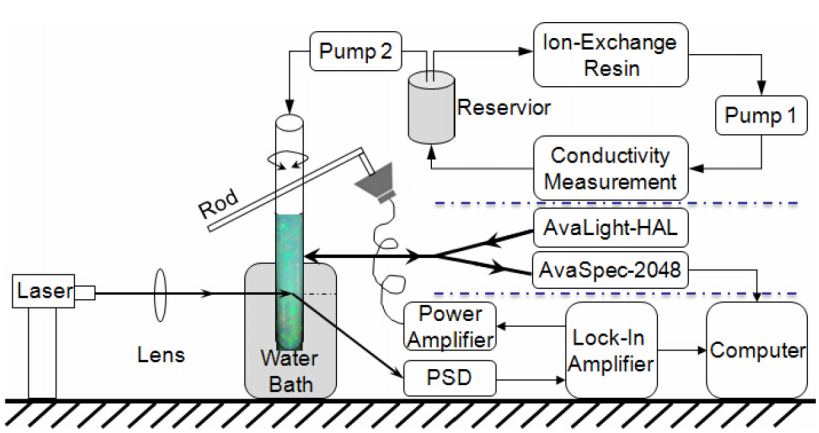

FIG. 1. Sketch of the experimental setup.

to identify crystal lattice structures and to collect light intensity corresponding to bcc and fcc in the bcc-fcc transition process.

3. Torsional resonance spectroscopy

This part was constructed according to some pioneering works.[31,32] Sinusoidal voltage signals generated from the oscillator of Lock-in amplifier (Signal Recovery 7230, Metek) is sent to the loudspeaker after power amplified. The membrane of the loudspeaker is connected to the rigid beam of cylindrical tube to make the tube vibrate synchronously. On the other hand, after passing through a lens, the incident laser hits the crystals and at positions satisfying Bragg's condition a bright band will be formed. Actually, this bright band is a small part of the first "Debye-Scherrer ring" from polycrystalline sample.[31] Shear waves generated by the oscillating tube wall will cause the interplanar distance of colloidal crystals to vary periodically and thus the position of the bright band, which is monitored by the position sensitive detector (PSD). Finally, voltage signals of PSD are fed back to Lock-in amplifier to pick out the resonance frequency after referencing with the out-put signals.

III. RESULTS AND DISCUSSIONS

A. Shear modulus measurement

For the coupled water-particle two component system driven by the oscillation of the cylindrical tube, the equation of motion had been founded and solved.[31,32,34] Shear modulus G of colloidal crystals can be measured by means of TRS. The periodic structure of crystals can form special constructive interference patterns when the Bragg's condition is satisfied. When the shearing force is applied to the crystals, the crystal structures are distorted causing the relevant pattern to vary accordingly and also the bright band position to displace. The displacement magnitude is determined by G. If the shearing force periodically oscillates, there will be a so-called resonance frequency ω at which the displacement magnitude reaches its maximum. G can be calculated through ω by

$$G = \frac{\omega_{jn}^2 \rho R^2}{\mu_j^2 + (n + 1/2)^2 \pi^2 \alpha^2}, \quad (1)$$

where R is the inner radius of the cylindrical vial, $\alpha = R/H$ is the aspect ratio between R and the filling height H, ρ is the mass density of the suspensions, and μ_j(=3.83, 7.01, 10.17, 13.32, . . .) are zeros of the first order Bessel function with $j = 1, 2, 3, 4, \ldots$ and $n = 0, 1, 2, 3, \ldots$ are the number of nodes of the vertical standing wave within the height H.

In order to test the effectiveness of TRS, PS105 with no bcc-fcc transition was used. The applied driving voltage on the loudspeaker was varied from 0.2 V, 0.5 V to 1.0 V, and the corresponding resonance spectra were shown in Fig. 2(a). Obviously, driving voltage has no influence on the locations of the resonance peaks. However, in order to avoid possible plastic flow, the driving voltages are usually small to ensure the lattice deformation is in the elastic limit. All the spectra clearly exhibit four resonance peaks, $\omega_{10}, \omega_{20}, \omega_{30}, \omega_{40}$, in the range of 0-30 Hz, and higher order frequencies are strongly damped by the suspending water. It should be mentioned that because the inner radius of the cylindrical vial R (4 mm) is much smaller than the filling height H (70 mm), $\alpha^2 = (R/H)^2 \approx 3.3 \times 10^{-3}$, so the term $(n + 1/2)^2 \pi^2 \alpha^2$ in Eq. (1) can be neglected. And then $\omega^2 - (\mu_j^2/\rho R^2)$ should have linear relationship, which is verified in Fig. 2(b). The value of shear modulus G can be calculated from the slope. However, for most cases only the first order resonance frequency ω_{10} should be enough.

B. Shear modulus in the process of bcc-fcc transition

For PS98, the phase behavior is more complicated. The suspensions begin to crystallize at volume fractions $\phi = 0.2\%$, where ϕ is proportion to particle concentration n. We found that the equilibrium stable structure is bcc for $\phi < 0.7\%$. For $\phi > 0.7\%$, though the thermodynamically stable structure is fcc, metastable bcc structure always appears first. With properly tuning ϕ and thus bcc-fcc transition rate, this system can be an appropriate candidate to investigate the shear modulus variation in the liquid-metastable(bcc)-stable(fcc) structure transformation process. By using the combination of TRS and RS,

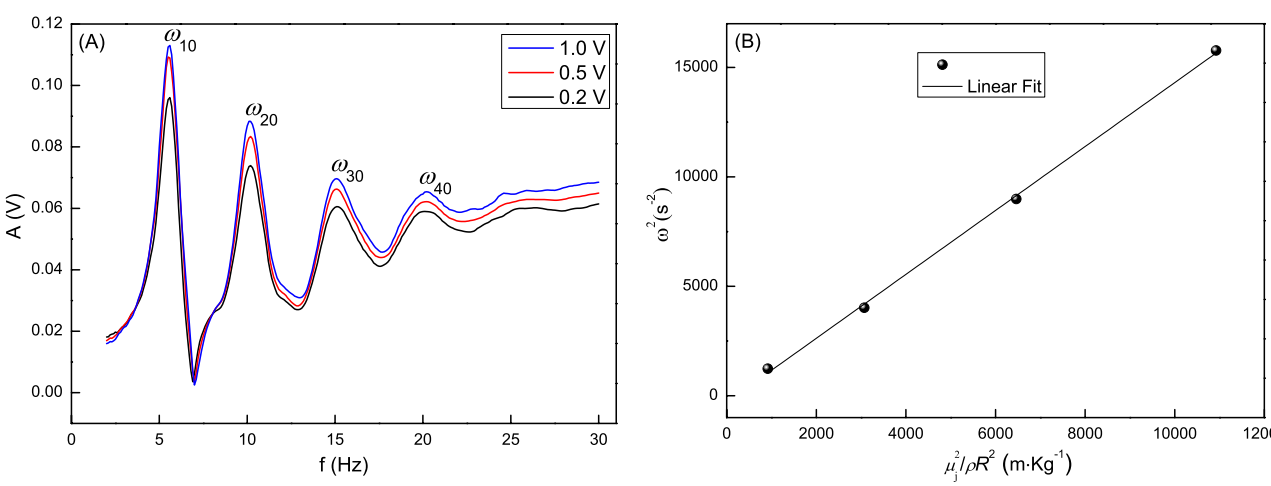

FIG. 2. (a) Resonance spectra obtained at different amplitude of driving voltages. (b) The relationship between $\omega^2 - (\mu_j^2/\rho R^2)$, G can be calculated from the slope.

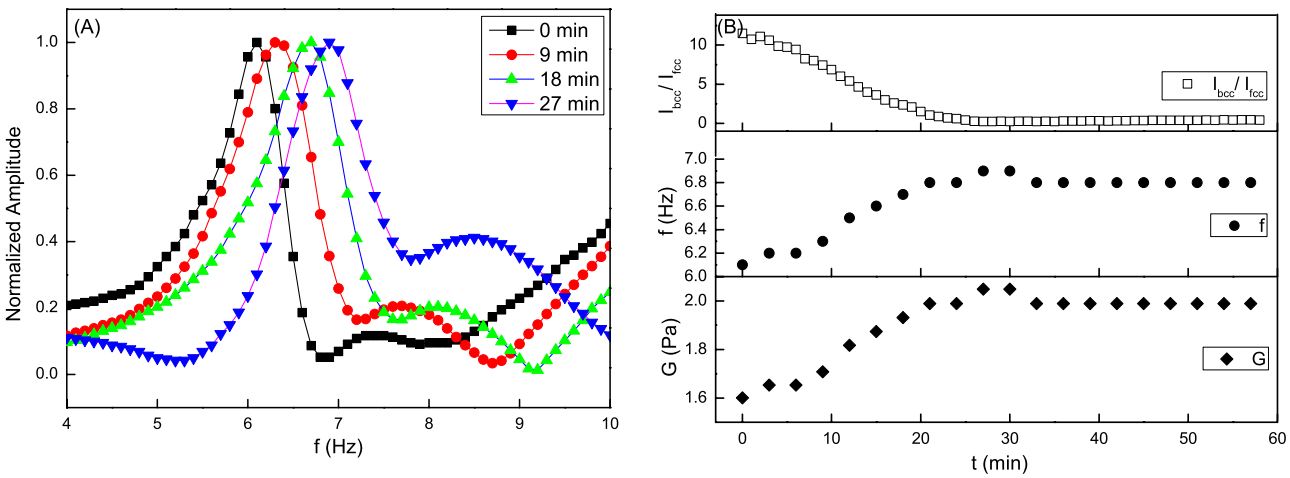

FIG. 3. (a) Resonance spectra collected at different transition time and (b) variation of I_{bcc}/I_{fcc}, f, and G during the structure transition process ($\phi = 1.03\%$).

we can synchronously obtain information about G and the corresponding structures of colloidal crystals during the structure transition.

The volume fractions ϕ used here are divided into two groups: one group (0.4%, 0.5%, 0.61%) is below the critical $\phi = 0.7\%$ and the other group (0.72%, 1.03%, 1.15%, 1.2%) is above it. For the first group, bcc is the stable state and G determined by TRS are 0.5, 0.8, 1.2 Pa, respectively. G increases with increasing ϕ, which is consistent with those reported in the literatures. The bcc-fcc transition rate increases with increasing ϕ. For instance, it took rather long time to make the bcc-fcc transition be completed for $\phi = 0.72\%$ but it spent less than 1 h to finish up the same transition process for $\phi = 1.03\%, 1.15\%, 1.2\%$.

For $\phi = 1.03\%$, resonance spectra recorded at different transition time were shown in Fig. 3(a). For the sake of brevity, only ω_{10} is given here. Clearly, the resonance frequency increases with the proceeding of bcc-fcc transition. Simultaneously, peak intensities of bcc (I_{bcc}) and fcc (I_{fcc}) were collected by RS, and the ratio of them, I_{bcc}/I_{fcc}, was used to represent the relative amount of bcc and fcc quantitatively. Specifically, the value of I_{bcc}/I_{fcc}, resonance frequency $f(=\omega/2\pi)$, and shear modulus G during the transition are shown in Fig. 3(b) from the top to the bottom. At the beginning, I_{bcc} is about one order of magnitude larger than I_{fcc}, which implies basically all the crystals are bcc at this stage. The resonance frequency is 6.1 Hz and the calculated shear modulus is 1.6 Pa. During the bcc-fcc transition, I_{bcc}/I_{fcc} decreases, but meanwhile f and G begin to increase. About 27 min later, I_{bcc}/I_{fcc} approaches to zero, indicating that all the metastable bcc has transformed into stable fcc and thus it is considered as the end of the transition. At this time, f and G reach their maximum values 6.8 Hz and 2.0 Pa. Namely, when crystal type changes from metastable bcc to stable fcc, G increases from 1.6 Pa to 2.0 Pa.

For the other two cases with $\phi = 1.15\%$ and 1.2%, the changing tendencies are similar to $\phi = 1.03\%$. But due to the bcc-fcc transition rate increases remarkably with increasing ϕ, the exact onset time is difficult to determine with accuracy. At the beginning, I_{bcc}/I_{fcc} is about 2.5 for $\phi = 1.15\%$ and 1.2 for $\phi = 1.2\%$, respectively (see Figs. 4(a) and 4(b)). Therefore, it is actually the mixture of untransformed metastable bcc and stable fcc at this moment, and the corresponding modulus of the system is assigned as G_{mixture}. G_{mixture} increases with increasing the amount of fcc, which indicates that at the very beginning of bcc-fcc transition the modulus of metastable bcc should be even smaller than G_{mixture} because there is no fcc at all at that time. And at the other end of the transition where metastable bcc disappears completely, G_{mixture} equals to the experimental G_{fcc}. In the case of stable fcc with $\phi = 1.15\%$

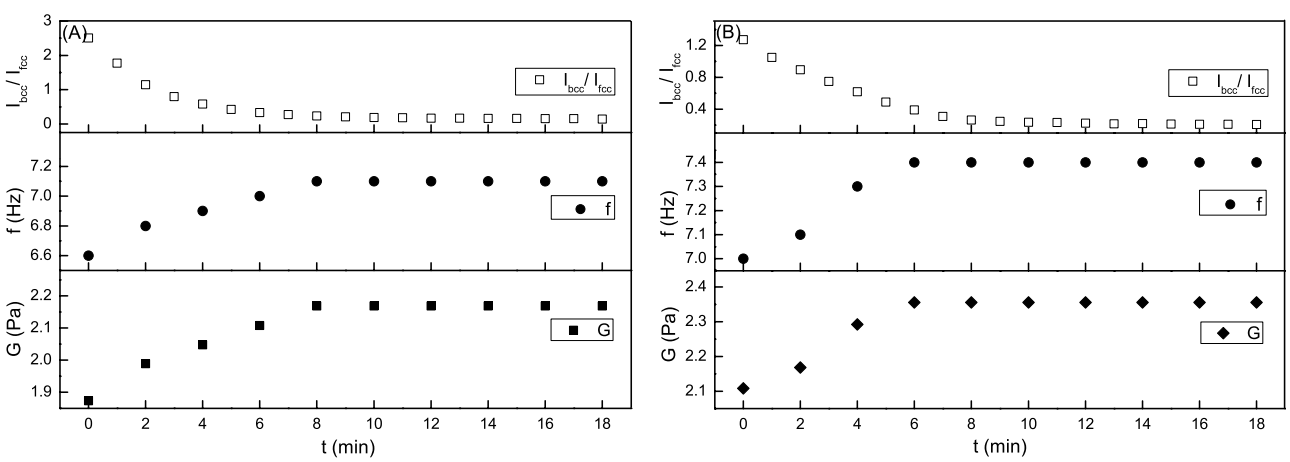

FIG. 4. Variations of I_{bcc}/I_{fcc}, f, and G during the bcc-fcc transition for (a) $\phi = 1.15\%$ and (b) $\phi = 1.2\%$.

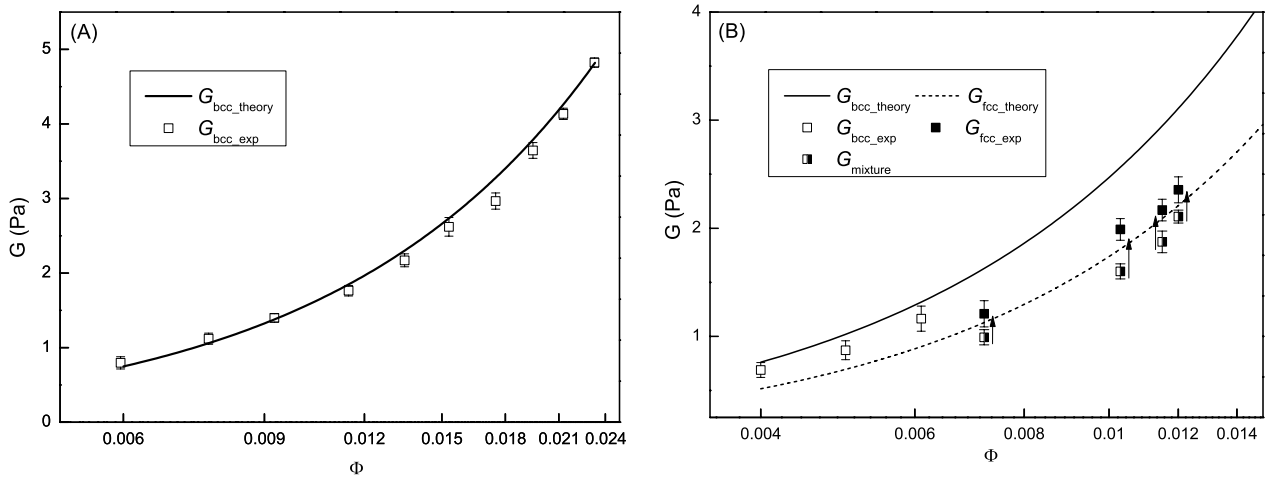

FIG. 5. Experimental and theoretical G-ϕ relationship of colloidal crystals. (a) PS105 with no bcc-fcc transition. All the crystals are bcc. (b) PS98 with bcc-fcc transition, the phase boundary is approximately at $\phi = 0.7\%$. Empty and filled square symbols are the experimental G of stable bcc and stable fcc, and the half-filled square symbols represent G of the mixtures of metastable bcc and stable fcc. Up arrows indicate the moduli increase during the bcc-fcc structure transition.

and 1.2%, their corresponding f and G are 7.1 Hz, 2.2 Pa and 7.4 Hz, 2.4 Pa, respectively.

C. Comparison between theoretical and experimental results

Theoretically, if the crystals are in thermodynamically stable state, their moduli can be derived from the interparticle interaction potential $V(r)$,[30,35]

$$G_{bcc} = f_A \frac{3\sqrt{3}}{4{d_{bcc}}^3}\left(\frac{4}{9}\frac{\partial^2 V(r)}{\partial r^2}\Big|_{r=d} d_{bcc}^2 + \frac{8}{9}\frac{\partial V(r)}{\partial r}\Big|_{r=d} d_{bcc}\right), \quad (2)$$

$$G_{fcc} = f_A \frac{\sqrt{2}}{{d_{fcc}}^3}\left(\frac{1}{2}\frac{\partial^2 V(r)}{\partial r^2}\Big|_{r=d} d_{fcc}^2 + \frac{3}{2}\frac{\partial V(r)}{\partial r}\Big|_{r=d} d_{fcc}\right), \quad (3)$$

where r is interparticle distance, d_{bcc} and d_{fcc} is the nearest neighbor distance of bcc and fcc, f_A is a numerical factor which accounts for the different boundary conditions in averaging over randomly oriented crystallites or local environs. Its theoretical limits are $f_A = 0.4$ for homogeneously distributed strains and $f_A = 0.6$ for homogeneously distributed stresses, respectively. For polycrystalline samples, however, $f_A = 0.5$ is encountered in most cases and will also be used here.[30]

For monodisperse charged colloidal system, the pair interaction potential $V(r)$ can be written as

$$V(r) = \frac{Z^2 e^2}{4\pi\varepsilon_0\varepsilon_r}\left(\frac{\exp(\kappa a)}{1+\kappa a}\right)^2 \frac{\exp(-\kappa r)}{r}. \quad (4)$$

In Eq. (4), Z is the effective charge number, e is the elementary charge, a is the particle radius, $\varepsilon_0\varepsilon_r$ is the dielectric permittivity of the suspensions, and κ is the inverse Debye-screening length given by

$$\kappa^2 = \frac{e^2}{\varepsilon_0\varepsilon_r k_B T}\left(nZ + 2000 N_A C_{salt}\right), \quad (5)$$

where n is the particle number density (m^{-3}, $\phi = n \cdot (4/3)\pi a^3$), C_{salt} is the molar concentration of the foreign salt (mol L^{-1}), N_A is Avogadro's constant, and $k_B T$ is the thermal energy. The first term in Eq. (5) represents the counterion contribution and the second term accounts for the excess electrolyte.

In practice, due to the accumulation of micro-ions around the charged particle surface and unavoidable contamination with air borne CO_2, effective charge number Z and actual salt concentration C_{salt} are hard to determine accurately; therefore, they can usually be obtained from the G-ϕ relationship by least squares fitting.[10] The fitted result is shown in Fig. 5(a) for PS105. Since the crystals are all bcc in the measured range of ϕ from 0.006 to 0.024 for PS105, Eq. (2) is used for fitting and we get $Z = 400 \pm 26$, $C_{salt} = 1.9 \times 10^{-6}$ mol L^{-1}. For PS98 with bcc-fcc transition (Fig. 5(b)), Eq. (3) and G-ϕ of stable fcc (filled squares) are used for fitting (dashed line) and the obtained values are $Z = 440 \pm 40$, $C_{salt} = 5 \times 10^{-7}$ mol L^{-1}, respectively. And then they are used to calculate the theoretical G_{bcc} (solid line) to compare with experimental values of bcc (empty squares).

From Fig. 5, we can see several points as below. (a) For pure bcc crystals with no bcc-fcc transition (PS105, Fig. 5(a)), G increases with the increasing of ϕ and it can be well expected by Eq. (2). (b) For suspensions with bcc-fcc transition (PS98, Fig. 5(b)), when the crystals reach their final stable structure, both in the region of stable bcc ($\phi = 0.4\%$, 0.5%, 0.61%) and stable fcc ($\phi = 0.72\%$, 1.03%, 1.15%, 1.2%), there is also good consistence between theoretical moduli and the experimental ones. (c) The moduli of the initial bcc extrapolated from the measurements should be smaller than $G_{mixture}$ and they are much smaller than theoretical G_{bcc}. Interestingly, they are even smaller than G_{fcc} under the same concentration, although theoretically the modulus for stable bcc should be much larger than that for stable fcc according to formula Eqs. (2) and (3) with the same parameters including the particle size, volume fractions, surface charge.

A possible reason for the lower shear modulus of the metastable bcc (more accurately, in the bcc-fcc transition) than that in the stable fcc phase is that crystalline imperfection due to not-well-equilibrated structure during the transition state. More specifically, the crystal lattices keep changing and particles on the lattice sites cannot effectively reach their

equilibrium positions in the transition state, and therefore its shear modulus becomes much smaller than theoretical expectations that are based on well-equilibrated structures. And the influence of crystalline imperfection is so large that the modulus is even smaller than that for perfect fcc structure. The full width at half maximum (FWHM) of RS may offer an evidence to somehow support the above explanation. According to Braggs' equation, the interplanar distance of colloidal crystals should be almost identical (when other influencing factors, such as thermal motions, are not considered) for a perfect crystal structure making FWHM smaller. The crystalline imperfection will make interplanar distance have an additional uncertainty resulting in a larger FWHM. Taking PS98 with ϕ = 1.03%, for instance, the values of FWHM for metastable bcc and stable fcc is 0.23 μm^{-1} and 0.15 μm^{-1}, respectively. Larger FWHM for metastable bcc should represent its crystalline imperfection.

IV. CONCLUSION

A combination of reflection spectrometer and torsional resonance spectroscopy was used to investigate the shear moduli variation in bcc-fcc transition. The experimental results are compared with theoretical formulas deduced from the microscopic interparticle interaction. In the range of ϕ where bcc is the stable state, theoretical values show good consistence with experimental ones. However, in the range of ϕ where fcc is the stable state but metastable bcc nucleates first, the shear modulus of the system increases obviously during the structure transition and it finally approaches to the maximum values after all the metastable bcc transformed into stable fcc. The current study confirms that in bcc-fcc transition the first formed bcc state has remarkably low mechanical strength than theoretical expectations. We attribute the low shear moduli to the high degree of defects and imperfections of crystalline in the bcc transient state.

ACKNOWLEDGMENTS

This work is supported by Grant Nos. 11302226, 11172302, and 11032011 from the National Natural Science Foundation of China (NNSFC). We greatly thank Mr. Da Zhang for the technical assistance in TRS setup.

[1]Y. Peng, F. Wang, Z. Wang, A. M. Alsayed, Z. Zhang, A. G. Yodh, and Y. Han, Nat. Mater. **14**, 101 (2015).
[2]P. J. Yunker, K. Chen, M. D. Gratale, M. A. Lohr, T. Still, and A. G. Yodh, Rep. Prog. Phys. **77**, 056601 (2014).
[3]P. Tan, N. Xu, and L. Xu, Nat. Phys. **10**, 73 (2014).
[4]T. Palberg, J. Phys.: Condens. Matter **26**, 333101 (2014).
[5]P. Wette and H. J. Schöpe, Phys. Rev. E **75**, 051405 (2007).
[6]I. A. Carlos, R. Edilso, and S. Andreas, Adv. Funct. Mater. **20**, 2565 (2010).
[7]Y. Takeoka, J. Mater. Chem. **22**, 23299 (2012).
[8]V. L. Alexeev, A. C. Sharma, A. V. Goponenko, S. Das, I. K. Lednev, C. S. Wilcox, D. N. Finegold, and S. A. Asher, Anal. Chem. **75**, 2316 (2003).
[9]P. J. Lu and D. A. Weitz, Annu. Rev. Condens. Matter Phys. **4**, 217 (2013).
[10]B. V. R. Tata and S. S. Jena, Solid State Commun. **139**, 562 (2006).
[11]A. Yethiraj, Soft Matter **3**, 1099 (2007).
[12]B. Liu, T. H. Besseling, M. Hermes, A. F. Demirors, A. Imhof, and A. van Blaaderen, Nat. Commun. **5**, 3092 (2014).
[13]A. Kuijk, T. Troppenz, L. Filion, A. Imhof, R. van Roij, M. Dijkstra, and A. van Blaaderen, Soft Matter **10**, 6249 (2014).
[14]Z. Zheng, F. Wang, and Y. Han, Phys. Rev. Lett. **107**, 065702 (2011).
[15]P. Pfleiderer and T. Schilling, Phys. Rev. E **75**, 020402 (2007).
[16]H. R. Vutukuri, F. Smallenburg, S. Badaire, A. Imhof, M. Dijkstra, and A. van Blaaderen, Soft Matter **10**, 9110 (2014).
[17]J. M. Meijer, D. V. Byelov, L. Rossi, A. Snigirev, I. Snigireva, A. P. Philipse, and A. V. Petukhov, Soft Matter **9**, 10729 (2013).
[18]P. Wette, H. J. Schope, and T. Palberg, J. Chem. Phys. **123**, 174902 (2005).
[19]P. Wette, A. Engelbrecht, R. Salh, I. Klassen, D. Menke, D. M. Herlach, S. V. Roth, and H. J. Schöpe, J. Phys.: Condens. Matter **21**, 464115 (2009).
[20]W. Hornfeck, D. Menke, M. Forthaus, S. Subatzus, M. Franke, H.-J. Schöpe, T. Palberg, J. Perlich, and D. Herlach, J. Chem. Phys. **141**, 214906 (2014).
[21]T. Palberg, J. Phys.: Condens. Matter **11**, R323 (1999).
[22]S. Xu, H. Zhou, Z. Sun, and J. Xie, Phys. Rev. E **82**, 010401 (2010).
[23]H. Zhou, S. Xu, Z. Sun, X. Du, and L. Liu, Langmuir **27**, 7439 (2011).
[24]K. Kratzer and A. Arnold, Soft Matter **11**, 2174 (2015).
[25]M. Santra, R. S. Singh, and B. Bagchi, J. Phys. Chem. B **117**, 13154 (2013).
[26]H. M. Lindsay and P. M. Chaikin, J. Chem. Phys. **76**, 3774 (1982).
[27]T. Okubo, J. Chem. Soc., Faraday Trans. **85**, 455 (1989).
[28]K. Ito, K. Sumaru, and N. Ise, Phys. Rev. B **46**, 3105 (1992).
[29]T. Palberg, J. Kottal, T. Loga, H. Hecht, E. Simnacher, F. Falcoz, and P. Leiderer, J. Phys. III **4**, 457 (1994).
[30]H. J. Schöpe, T. Decker, and T. Palberg, J. Chem. Phys. **109**, 10068 (1998).
[31]E. Duboisviolette, P. Pieranski, F. Rothen, and L. Strzelecki, J. Phys. **41**, 369 (1980).
[32]M. Joanicot, M. Jorand, P. Pieranski, and F. Rothen, J. Phys. **45**, 1413 (1984).
[33]H. Zhou, S. Xu, W. Ouyang, Z. Sun, and L. Liu, J. Chem. Phys. **139**, 064904 (2013).
[34]J. F. Joanny, J. Colloid Interface Sci. **71**, 622 (1979).
[35]R. A. Johnson, Phys. Rev. B **6**, 2094 (1972).